Diffusion in complex ordered alloys: Atomic-scale investigation of $NiAl_3$

David Tingaud* and Françoise Nardou†
Laboratoire de Science des Procédés Céramiques et Traitements de Surface, CNRS UMR 6638, Université de Limoges, 123 Avenue Albert Thomas, 87060 Limoges Cedex, France

Rémy Besson‡
Laboratoire de Métallurgie Physique et Génie des Matériaux, CNRS UMR 8517, Université des Sciences et Technologies de Lille, Bâtiment C6, 59655 Villeneuve d'Ascq Cedex, France

(Received 18 February 2010; revised manuscript received 21 April 2010; published 12 May 2010)

Although involved in most solid-state processes, ordered compounds are often characterized by complex crystallographies and chemical properties, which drastically restricts the range of experimental investigations, and urges more realistic simulation frameworks. Considering the case of $NiAl_3$ and the unknown diffusion properties of its practically important cementite-type structure, we use embedded-atom-method-based atomic-scale simulations to perform a detailed analysis of its kinetic parameters controlling jump rates, including migration profiles, saddle points and attempt frequencies. The global approach proposed here is made necessary by the intricate coupling between these quantities, which rules out more usual schemes relying on selected transitions. It provides the required material for atomistic simulations of diffusion in low-symmetry ordered phases.

DOI: 10.1103/PhysRevB.81.174108 PACS number(s): 61.72.Bb

I. INTRODUCTION

Due to their importance in solid-state transformations,[1] the diffusion properties of the various intermetallic phases involved in practical processes constitute a topic of utmost interest. Although highly valuable, in principle, experimental approaches are not well suited to deal with this issue, since the properties of ordered alloys depend strongly on composition, a parameter often controlled with insufficient accuracy in experiments. Devising efficient phase-transformation predictive tools requires a detailed knowledge of the diffusion properties as functions of the thermodynamic variables, a goal that can be more conveniently achieved through theoretical approaches. To this purpose, while the increase in performance of computers may initiate to resort massively to simulations, the tractability requirement of such procedures generally implies the selection of a restricted pool of *a priori* postulated atomic transitions. Such hypotheses may be critical for the frequently intricate crystallographies and chemistries of ordered compounds, hence such "all-simulation" schemes in practice are employed mostly for cubic disordered alloys. With intermetallic phases, conversely, it may be fruitful to analyze the diffusion properties on analytic grounds: such a point of view can be used even in complex situations (reduced symmetry, multicomponent alloys with additions[2]), and is also a convenient way to investigate the influences of the various mechanisms entering a net diffusion coefficient.

In this context, the Al-Ni system, of wide application fields,[1] has been extensively studied on its Ni-rich side, especially as regards B2 NiAl and $L1_2$ Ni_3Al. On the contrary, Al-rich nickel aluminides are still poorly investigated, partly due to their low melting point and to the difficulties associated with their synthesis. However, these phases have recently received further attention from experimentalists, owing to their potential advantages for structural or functional applications.[3,4] In addition, aluminum-rich Ni-Al alloys are experimentally known[5–7] to appear transiently in solid-state processes. Therefore, since the final properties are governed by transient states, it is relevant to investigate the properties of such intermediate phases as $NiAl_3$ and Ni_2Al_3.

Special attention should be paid to $NiAl_3$, a line compound in a narrow range of composition below 1100 K, crystallizing in the practically important, yet widely unknown, cementite-type $D0_{11}$ structure. Because of its complex crystallography, few theoretical works have been carried out on this ordered alloy, only available being a study of its structural, electronic, and optical properties[8] based on a full-potential linearized augmented plane-wave method, and an investigation of its defect thermodynamics within a pseudopotential approximation.[9]

Attempting to go one step further into the field of complex intermetallic phases, the present paper aims at providing an atomic-scale study of the diffusion properties of $NiAl_3$, with emphasis laid on methodological aspects possibly critical for low-symmetry ordered phases. As mentioned above, dealing with such phases involves a thorough analysis of all ingredients combining to yield the net diffusion coefficients, namely, the point defects[2] and their relation with the atomic transitions, together with a reasonable description of migration energies and jump frequencies. In spite of their current limitations, empirical interatomic potentials are still the only tractable way to perform this task, and will therefore be employed here. Their simplicity allows to refine the analysis along several lines (and far beyond the current possibilities of up-to-date *ab initio* methods), exploring: (i) a wide range of atomic transitions, (ii) the full migration energy and attempt frequency spectra, including local effects usually overlooked though important in intermetallics, such as saddle-point pressures[10] and point-defect phonons.[11–15]

II. METHODOLOGY

The $NiAl_3$ orthorhombic unit cell, oP16 or $D0_{11}$ cementite, space-group *Pnma* (Fig. 1), contains 4 Ni and 12 Al

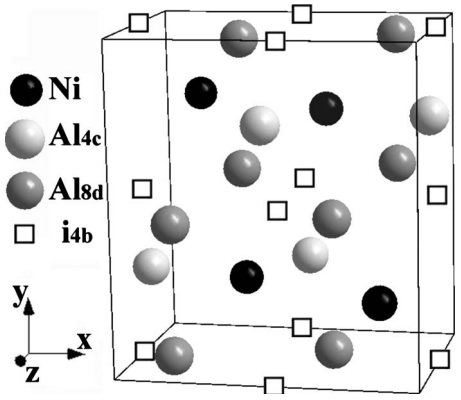

FIG. 1. Orthorhombic unit cell of $D0_{11}$ $NiAl_3$.

atoms, with two nonequivalent positions for the latter. The three sublattices (also named 1, 2, and 3 for brevity) are, respectively, labeled in Wyckoff notation as $(4c;8d)$ for Al and $4c$ for Ni. In addition, a previous work on $NiAl_3$ (Ref. 9) has pointed out the importance of $4b$ interstitial sites, located in $(\frac{1}{2}\frac{1}{2}0)$, $(\frac{1}{2}00)$, $(0\frac{1}{2}\frac{1}{2})$, $(00\frac{1}{2})$, hence an eight-element set of point defects, $[V_{\mathrm{Al}(8d)}$, $V_{\mathrm{Al}(4c)}$, $V_{\mathrm{Ni}(4c)}$, $\mathrm{Al}_{\mathrm{Ni}(4c)}$, $\mathrm{Ni}_{\mathrm{Al}(8d)}$, $\mathrm{Ni}_{\mathrm{Al}(4c)}$, $\mathrm{Al}_{i(4b)}$, and $\mathrm{Ni}_{i(4b)}]$, which provides the basis for a diffusion model, together with the hypothesis of atom-vacancy exchanges between the various pairs of sublattices. Although somewhat restricting, in principle, this framework may be reasonably accepted for $NiAl_3$, since the low symmetry should reduce the effect of correlation between jumps, making improbable strongly correlated sequences such as, for instance, the well-known "six-jump cycles" postulated in structures (such as B2) with higher symmetries. Moreover, a neighbor analysis using standard site positions[16] reveals the existence, for each sublattice pair, of a distance "gap" for the neighbor shells. This feature suggests to restrict (without loss of generality) the family of atom-vacancy exchanges to those contained within this cutoff distance, leaving a working set of 33 atomic transitions for each species. Throughout this paper, all jumps for species X (=Ni, Al) will be labeled as sl_1-sl_2_$pN(X)$, sl_1 and sl_2 being the initial and final sublattices for the vacancy, the atom moving thus in reverse direction, and p being the neighbor subshell inside sl_1-sl_2 (according to the positions specified in Ref. 16).

Due to the practical importance of these intermetallics, several N-body [embedded-atom-method (EAM)] empirical force fields have been constructed for NiAl or Ni_3Al by different groups,[17–19] but none was especially dedicated to the Al-rich part of the Al-Ni system, and these potentials fail to describe $NiAl_3$. For example, with the model presented in Ref. 17, frequently used to calculate the properties of Ni_3Al, the $NiAl_3$ compound crystallizes in tetragonal form instead of the correct orthorhombic $D0_{11}$ structure. On the contrary, a recent potential[20] allowed the less common Al-Ni phases ($NiAl_3$, Ni_2Al_3, or Ni_5Al_3) to be modeled with a notably higher accuracy, hence its selection in the present work. The use of an empirical potential for a point defect and diffusion study enables to use simulation supercells large enough to ensure reasonable convergence: here, the point-defect energies, harmonic (HA) calculations (energy minima or saddle points) and migration energies involved $10\times10\times10$, $4\times4\times4$, and $5\times5\times6$ $D0_{11}$ unit cells, respectively. Furthermore, in all harmonic calculations, a single k point was used to calculate the various free energies, the results being unaltered by grid refinements.

TABLE I. Comparison of the HA and QHA for point-defect GC entropies (S^{vib}_{GC}, k_B units) in B2 NiAl, using the same empirical potential (Ref. 20) (values at $T=1000$ K).

Defect	QHA (Ref. 20)	HA (this work)
$\mathrm{Al}_{\mathrm{Ni}}$	0.066	0.013
$\mathrm{Ni}_{\mathrm{Al}}$	4.837	4.827
V_{Al}	−2.721	−2.733
V_{Ni}	−6.935	−6.949

Throughout this work, the point-defect properties of the compound were determined within the grand-canonical (GC) formalism[21,22] of the independent-point-defect approximation. This method, the only one tractable for complex crystallographies,[2] can be extended straightforwardly to include the effect of vibrations, as the latter were previously shown to be non-negligible in $NiAl_3$.[23] F_0 being the free energy of the reference (undefected) system and $F(d)$ that pertaining to a single defect d, the key parameters under zero external pressure are the set of point-defect GC free energies,

$$F_{\mathrm{GC}}(d) = F(d) - F_0 \tag{1}$$

equivalently written as (isolating the $T=0$ K, vibration energy and vibration entropy contributions) for defect d,

$$F_{\mathrm{GC}} = E^0_{\mathrm{GC}} + E^{vib}_{\mathrm{GC}}(T) - TS^{vib}_{\mathrm{GC}}(T). \tag{2}$$

In order to evaluate the phonon corrections to point-defect GC free energies and jump rates, we used the strictly harmonic approximation (HA), namely, the $T=0$ K relaxed volumes around the defects, without quasiharmonic optimization (QHA) of these volumes. This restriction (practically unavoidable in order to maintain tractability) should not be critical, as both methods are found (Table I) to yield almost identical results for B2 NiAl (with the same EAM potential[20]). In the B2 compound, the largest HA-QHA discrepancy, occurring for Al antisites, only amounts to correcting the TS_{GC} term for this defect by less than 5 meV at 1000 K, which exceeds the precision limit of the empirical potential.

Within the activated state theory, the migration profiles were calculated preferentially via the "constrained atom" (CA) method, since the latter (also called "drag" method[14]), of easy handling, was particularly suited for the large number of atomic transitions available in $NiAl_3$, and is reputed sufficient for most transitions involving a single particle. For $NiAl_3$ however, the CA method revealed deficiencies in several cases, imposing the "nudged elastic band" (NEB) method.[24] While the latter usually involved a large set (30) of "images," this number, however, had to be reduced (down to 18) in few cases, in order to avoid unexpected behaviors (image glide along energy profiles) impairing the determination of the saddle-point position. Moreover, the effective location of the saddle point was sometimes found to require

TABLE II. GC free-energy parameters of point defects in $NiAl_3$ (EAM calculations): $T=0$ K energies, together with $T=800$ K vibration energies, entropic terms, and free energies (eV).

	Al($4c$) sites		Al($8d$) sites		Ni($4c$) sites		i($4b$) interstitial sites	
	V_{Al}	Ni_{Al}	V_{Al}	Ni_{Al}	V_{Ni}	Al_{Ni}	Al_i	Ni_i
E^0_{GC}	5.17	−0.60	4.90	−1.19	6.00	3.56	−1.20	−4.62
E^{vib}_{GC}	−0.21	0.00	−0.21	0.00	−0.21	0.00	0.21	0.21
$-TS^{vib}_{GC}$	0.26	−0.34	0.20	−0.20	0.33	−0.23	−0.76	−0.78
F^{vib}_{GC}	0.05	−0.34	−0.01	−0.20	0.12	−0.23	−0.55	−0.57

nonstandard refinements (see below), a feature probably specific to low-symmetry environments.

The pool of CA- or NEB-estimated saddle points was then used as an input for the harmonic analysis required to determine the jump attempt frequency spectrum of the compound. It is important to note that, although saddle-point pressures are known to have little influence on migration energies, they may nevertheless correspond to significant modifications of the attempt frequencies[10,25]), hence of the jump rates. More precisely, the practical atomic-scale simulation of a $1\rightarrow 2$ jump passing through an activated state $*$ provides the jump rate $\gamma^{1\rightarrow 2}_{NVT}(V_a,T)$ at constant volume V_a, whereas this transition more realistically occurs at constant pressure P_b, with a jump rate $\gamma^{1\rightarrow 2}_{NPT}(P_b,T)$, both quantities being related by

$$\gamma^{1\rightarrow 2}_{NPT}(P_b,T)=\gamma^{1\rightarrow 2}_{NVT}(V_a,T)e^{-P_bV_m(P_b)/k_BT}e^{\beta V_a[P^*_a-P^1_a]/k_B} \quad (3)$$

with V_m the migration volume at constant pressure P_b, and (P^1_a,P^*_a) the pressures in states 1 and $*$ at volume V_a. The same correction holds for the attempt frequencies, namely,

$$\tilde{\nu}^{1\rightarrow 2}_{att}=\nu^{1\rightarrow 2}_{att}e^{-P_bV_m(P_b)/k_BT}e^{\beta V_a[P^*_a-P^1_a]/k_B}, \quad (4)$$

where $\nu^{1\rightarrow 2}_{att}$ and $\tilde{\nu}^{1\rightarrow 2}_{att}$ are, respectively, the "raw" (constant volume) and "P-corrected" (constant-pressure) attempt frequencies for the jump. This yields a physically sound jump rate of the form $\gamma^{1\rightarrow 2}_{NPT}=\tilde{\nu}^{1\rightarrow 2}_{att}e^{-E_m/k_BT}$ (with E_m the migration energy). Expression (4) will be used throughout below, with $P_b=P^1_a=0$ (system under $P=0$ at equilibrium), involving therefore only saddle-point residual pressures. The coefficient $\beta=\frac{1}{V}(\frac{\partial V}{\partial T})_P=-\frac{1}{V}(\frac{\partial S}{\partial P})_T$ is the isothermal compressibility of the perfect crystal, a unique value being assumed to pertain to states 1, 2, and $*$ (in the present case, $\beta=4.51\times 10^{-5}$ K^{-1}, quasi-independent of temperature, was obtained consistently using the same EAM potential).

III. DETERMINATION OF KINETIC PARAMETERS

A. Point defects

As mentioned above, investigating point defects in complex intermetallics can be conveniently achieved through the independent-point-defect approximation,[2] provided the composition-temperature domain of validity of this hypothesis is sufficiently wide (a reasonable assumption except in case of strong defect clustering). The GC parameters of point defects in $NiAl_3$ and their formation energies at 0 K around stoichiometry are displayed, respectively, in Tables II and III. For purpose of comparison, Table III also presents the results of a similar investigation in $NiAl_3$ with a pseudopotential density-functional theory (DFT) method.[9] The agreement between EAM and DFT calculations is satisfactory for the $x_{Ni}=0.25$ compound, and the same constitutional defects (zero formation energies, i.e., lowest point-defect excitations) are also obtained on each side of stoichiometry, respectively, $Ni_{Al(8d)}$ and $V_{Ni(4c)}$ for Ni and Al excess. Moreover, in spite of a lower EAM value, both approaches agree to favor interstitial Ni for $x_{Ni}>0.25$. The EAM model thus predicts with reasonable accuracy the properties of most

TABLE III. $T=0$ K formation energies of point defects in $NiAl_3$, at and on both sides of stoichiometry, from EAM (this work) and DFT (Ref. 9) calculations.

	$x_{Ni}<0.25$		$x_{Ni}=0.25$		$x_{Ni}>0.25$	
	EAM	DFT	EAM	DFT	EAM	DFT
$V_{Al(4c)}$	1.95	1.90	1.72	1.56	1.55	1.29
$Ni_{Al(4c)}$	2.18	2.90	1.27	1.50	0.59	0.45
$V_{Al(8d)}$	1.68	1.90	1.45	1.55	1.28	1.29
$Ni_{Al(8d)}$	1.59	2.44	0.68	1.05	0.00	0.00
$V_{Ni(4c)}$	0.00	0.00	0.68	1.05	1.19	1.83
$Al_{Ni(4c)}$	0.77	0.61	1.69	2.01	2.37	3.06
$Al_{i(4b)}$	2.02		2.25		2.42	
$Ni_{i(4b)}$	1.38	2.22	0.70	1.18	0.19	0.39

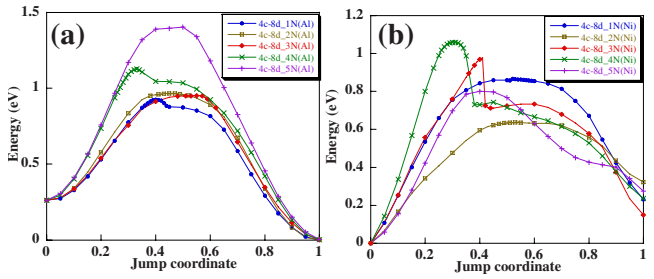

FIG. 2. (Color online) Jump profiles of increasing neighborhood (1N-5N) for (a) Al and (b) Ni atoms between $4c$ (=1) and $8d$ (=2) sublattices in $NiAl_3$ (EAM calculations with CA method).

types of point defects, its main deficiency being the overstabilization of some secondary defect species. The high-energy cost of aluminum vacancies seems to be a usual feature of this kind of point defect, and is probably associated with structural instabilities (see below), already detected not only in other nickel aluminides such as NiAl (Ref. 14) and Ni_2Al_3,[26] but also in FeAl (Ref. 27) or in pure Al.[28] Thus, from this point-defect analysis, and in spite of accuracy limits inherent to fitted empirical models, the EAM potential of Ref. 20 appears as suitable for the study of diffusion in $NiAl_3$.

Considering the effect of point-defect phonons, the contribution of each term of Eq. (2) (energy and entropy) in $NiAl_3$ is detailed in Table II. While for vacancies and interstitials both the entropy and energy terms contribute, E_{GC}^{vib} is close to zero for antisites, in agreement with previous works.[15] On the whole, dealing with defect free energies (F_{GC} instead of E_{GC}^{0}) leads to a strong softening of the defect-composition profiles, which clearly evidences the role of point defect phonons in $NiAl_3$. As a consequence, the amount of interstitial Al, although lower than that of $Ni_{i(4b)}$, may not be negligible in $NiAl_3$. However, using the same EAM potential, further analysis also reveals that interstitial Al atoms in $NiAl_3$ form doublets [contrary to Ni, which occupies a single $i(4b)$ site] similar to the well-known dumbbells observed in iron alloys. This may be a hint of more complex interstitial Al defects with possibly associated collective atomic movements. These issues however deserve confirmation, and the consequence in the present work is simply to discard Al interstitial diffusion, the latter being allowed only for Ni.

B. Transition paths

Relying on the previous point-defect analysis, the next step toward diffusion properties consists in a detailed investigation of atomic migration, based on the aforementioned hypothesis of atom-vacancy exchange mechanisms. Inspection of the various transition profiles reveals that the atomic jumps in $NiAl_3$ can be divided into two classes, according to topological features of the energy landscape. As a first set, all transitions involving only the Al (1=$4c$ and 2=$8d$) sublattices are characterized by a reaction coordinate, and thus can be easily obtained using the CA method. The resulting energy profiles are displayed on Fig. 2, illustrating the case of mixed $Al(4c) \leftrightarrow Al(8d)$ jumps. Although a small part of them shows a somewhat steep shape, this does not constitute an obstacle to the localization of the saddle point, as confirmed by the harmonic analysis easily providing the single required imaginary eigenfrequency for each jump. It should also be noted that the value of this frequency is moderately sensitive ($<20\%$) to the precise position around the saddle point. As shown by Fig. 2, the migration energy does not simply increase with the jump length, and a distance criterion for the selection of jumps should therefore not be valid in complex crystallographies. Al and Ni jumps show quite similar behaviors ($E_m < 1.5$ eV), which *a priori* suggests that the Al($4c$) and Al($8d$) sublattices should be favorable to the diffusion of both chemical species (this point will be discussed below).

The situation drastically changes with jumps involving either the Ni($4c$) or interstitial ($4b$) sublattices (=3,4). A wide set of such transitions have to be discarded due to athermal instabilities, namely, (i) all $Al(4c) \leftrightarrow Ni(4c)$ and $Al(8d) \leftrightarrow Ni(4c)$ jumps for Al, (ii) all $Al(4c) \leftrightarrow i(4b)$ and $Al(8d) \leftrightarrow i(4b)$ jumps for both species. Case (i) corresponds to a spontaneous recombination of Al vacancies with neighboring antisite Al toward a single Ni vacancy. Such processes were already noted in other aluminides[27] with much simpler (B2) structures, either modeled with empirical potentials or *ab initio* methods, and may therefore be characteristic of the chemical bonding between normal and transition metals, irrespective of the local symmetry of the lattice. As for case (ii), it also corresponds to an instability of the Al vacancy, this time in presence of interstitials of any chemical type. It therefore rules out the possibility of mixed jumps involving $i(4b)$ and Al($4c$) or Al($8d$) sites, leaving $Ni(4c) \leftrightarrow i(4b)$ transitions as the only possibility. The investigation of such instabilities in other compounds with $D0_{11}$ cementite structure (especially Fe_3C) would be valuable.

Moreover, in contrast with the situation depicted for $Al(4c)/Al(8d)$ sublattices, $Ni(4c)/i(4b)$ jumps cannot be efficiently investigated with the CA method. The latter systematically yields discontinuous energy profiles, indicating nonmonotonic migration paths with respect to the reaction coordinate. As a consequence, the CA method is found to miss the saddle point for most jumps of this class, as confirmed by the emergence of a second spurious imaginary eigenvalue. This unsatisfactory behavior is somewhat surprising, as it appears in transitions involving only a single atom, and may therefore be due to the complex topology of the energy landscape of the $D0_{11}$ structure. Conversely, the NEB method is found to yield smooth profiles throughout, the contrasting behaviors of both methods being illustrated on Fig. 3 for the 3–3_2N Al jump. This confirms that in low-symmetry cases such as $D0_{11}$, CA methods may lead to critical underestimations of migration barriers, while NEB profiles are sufficient to assess such quantities within 10^{-2} eV, a reasonable precision with an empirical energy model.

C. Saddle-point localization

Compared to energy barrier calculations, jump frequencies require an enhanced precision in the localization of

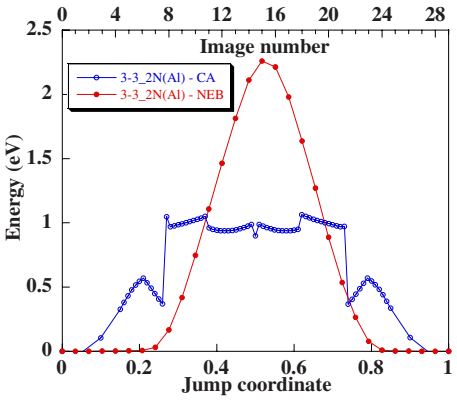

FIG. 3. (Color online) EAM profiles for Al second-neighbor jump within Ni($4c$) (=3) sublattice in $NiAl_3$: comparison of the CA and NEB methods.

saddle points, which cannot always be easily achieved, even using various interpolation schemes of the atomic positions[24] or dedicated flavours[29] of the NEB method. For instance, due to persistent "image glide," a NEB refinement of the seemingly simple profile of Fig. 3 was not sufficient to reach the saddle point with accuracy. As complex crystallographies are associated with numerous inequivalent jumps, thus possibly prone to similar shortcomings, it may be relevant to propose here an alternative route, namely, a "normal-mode analysis" (NMA) consisting of iterative displacements in direction of energy extrema along selected normal modes.

To illustrate this approach, it is instructive to consider the aforementioned 3–3_2N Al jump, unexpectedly crippled with a spurious second imaginary mode. The NMA initial state, related to the NEB-estimated saddle point (image 15 of Fig. 3), is depicted in Fig. 4(a) which displays the energy profiles along both imaginary modes (for clarity, each mode is labeled on the graphs). Although globally convex, the profile along the secondary mode (N=2400) is locally flat with a shallow inverse concavity responsible for the spurious behavior, which emphasizes the complexity of the $D0_{11}$ energy landscape. The main imaginary mode (N=2306) shows a non-negligible offset of its maximum with respect to the origin of the normal coordinate (q) axis, a deficiency readily remedied via a first iteration, bringing the system to the point q_{2306}=0.7 [Fig. 4(b)]. Iteration 1 however does not eliminate the local concavity of the secondary profile (N=2364), hence a new iteration along this mode, leading to q_{2364}=2.5 [Fig. 4(c)]. The second imaginary mode is maintained, but the larger slope suggests a configuration closer to the saddle point, which is confirmed by a third iteration (leading to q_{2355}=3.2) removing the spurious mode [Fig. 4(d)]. Applying NMA, it should be noted that the choice of which (principal or secondary) imaginary mode is selected, may vary from one iteration to another (it may also depend on the jump considered). Finally, our study strongly suggests that, in complex crystallographies such as $D0_{11}$, an accurate localization of saddle points may require dedicated (normal-mode) analyses, beyond standard NEB procedures, somewhat restricting the search to tractable energy models (EAM potentials for metals, empirical force fields for ionic solids,…) and leaving it currently beyond the scope of *ab initio* calculations.

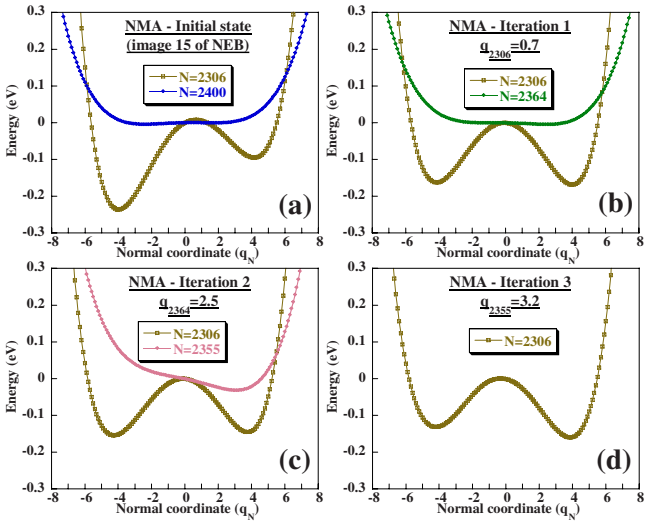

FIG. 4. (Color online) NMA around the NEB-estimated saddle point (image 15 of Fig. 3) for the second-neighbor jump of Al within Ni($4c$) sublattice.

D. Jump attempt frequencies

Controlling matter transport, the jump attempt frequency spectrum is the last feature that requires careful investigation in a complex ordered compound such as $D0_{11}$ $NiAl_3$. As shown elsewhere[10] and recalled above, jump frequencies must necessarily be corrected using saddle-point pressures. This correction is essential to ensure realistic results, since it provides for each attempt frequency a nonambiguous value, independent of the somewhat arbitrary volume used in a raw constant-volume calculation of eigenfrequencies: using the notations of relation (4), the efficiency of the correction lies in that the set of $\{\nu_{att}\}$ relative to various arbitrary volumes converge toward a unique, physically much more meaningful $\tilde{\nu}_{att}$ value. For the whole set of atomic transitions considered in this work, the $(E_m, \tilde{\nu}_{att})$ spectra obtained along these lines are gathered in Table IV. For the sake of clarity, jumps involving Ni($4c$) or $i(4b)$ sites are presented separately from those confined within the Al($4c$) and Al($8d$) sublattices. The transition parameters of jumps confined to both Al sublattices are weakly dependent on the neighbor shell with values for Al (respectively, Ni) $\tilde{\nu}_{att}$ close to the upper (respectively, lower) part of the phonon spectrum of the compound. While a similar tendency is detected for jumps connecting the Ni($4c$) and either Al sublattice, a much different behavior is obtained for jumps confined to Ni($4c$) and $i(4b)$, with values exceeding 10^4 THz. On the whole, the P-corrected $\tilde{\nu}_{att}$ spectrum is wide, ranging over 5 orders of magnitude (roughly between 0.1 and 1000 THz), which confirms the inadequacy of employing more or less generic attempt frequencies for a realistic diffusion study in complex ordered phases. Another remarkable feature of the data of Table IV, especially evidenced for $[\mathrm{Ni}(4c);i(4b)]\leftrightarrow[\mathrm{Ni}(4c);i(4b)]$ jumps, is the compensation effect between increasing E_m and $\tilde{\nu}_{att}$, which rules out schemes relying solely on lower migration energies,

TABLE IV. Spectra of P-corrected attempt frequencies (THz) and migration energies (eV) in $NiAl_3$: (a) jumps within Al($4c$) and Al($8d$) sublattices, (b) jumps involving Ni($4c$) or i($4b$) sublattices.

Transition	$\tilde{\nu}_{att}$	E_m	Transition	$\tilde{\nu}_{att}$	E_m
		(a) Al($4c$) and Al($8d$)			
1–1_1N(Al)	427	2.17	1–1_1N(Ni)	0.2	0.88
2N(Al)	1098	2.50	2N(Ni)	2	1.20
1–2_1N(Al)	32	0.66	1–2_1N(Ni)	4	0.86
2N(Al)	29	0.70	2N(Ni)	7	0.64
3N(Al)	56	0.69	3N(Ni)	17	0.98
4N(Al)	56	0.87	4N(Ni)	20	1.06
5N(Al)	114	1.14	5N(Ni)	8	0.80
2–1_1N(Al)	14	0.93	2–1_1N(Ni)	0.3	0.64
2N(Al)	13	0.97	2N(Ni)	0.4	0.31
3N(Al)	24	0.95	3N(Ni)	1	0.83
4N(Al)	24	1.13	4N(Ni)	1	0.82
5N(Al)	49	1.40	5N(Ni)	0.5	0.53
2–2_1N(Al)	14	0.44	2–2_1N(Ni)	6	0.96
2N(Al)	42	0.81	2N(Ni)	27	1.09
3N(Al)	76	0.87	3N(Ni)	10	0.78
		(b) Ni($4c$) or i($4b$)			
1–3_1N(Ni)	6	0.51	3–3_1N(Al)	50088	2.64
2N(Ni)	4	0.39	2N(Al)	5717	2.26
3N(Ni)	18	0.98	3N(Al)	7613	2.05
3–1_1N(Ni)	1	0.49	3–3_1N(Ni)	15864	2.95
2N(Ni)	0.3	0.27	2N(Ni)	12799	3.13
3N(Ni)	0.8	0.91	3N(Ni)	22	2.13
2–3_1N(Ni)	4	0.39	3–4_1N(Ni)	7	0.31
2N(Ni)	8	0.73	4–3_1N(Ni)	614	1.68
3N(Ni)	4	0.30	4–4_1N(Ni)	55	1.36
3–2_1N(Ni)	2	0.51			
2N(Ni)	8	1.07			
3N(Ni)	2	0.50			

and demonstrates that an overall analysis is required when investigating diffusion in low-symmetry intermetallic phases.

IV. DISCUSSION: DIFFUSION IN $D0_{11}$ $NiAl_3$

As it provides the parameters monitoring jump rates, the foregoing analysis is adapted to further "direct" atomistic (for instance, kinetic Monte Carlo) simulations of the diffusion properties of $NiAl_3$. Combined with further modeling of correlation effects, such investigations would probably be very fruitful. However, leaving this for future work, we use here the point-defect based analytical formulation[30] of a tracer diffusion coefficient, which readily allows to obtain this quantity as a function of the Ni content. Concentrating on the y-axis diagonal component and $T=800$ K (a temperature compatible with the existence of Al-rich phases in the elaboration processes of Ni-Al alloys), Fig. 5 thus gives an insight into the "diffusion landscape" of a $D0_{11}$ compound.

Both species are found to have very dissimilar diffusion properties, Ni being five orders of magnitude more mobile than Al. This is related to the dominant mechanisms for matter transport, which differ significantly between Al and Ni.

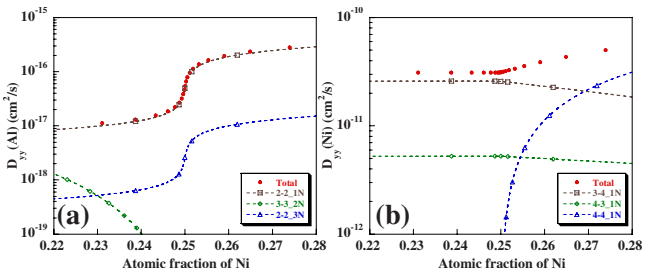

FIG. 5. (Color online) Tracer diffusion coefficients (D_{yy} components) in $NiAl_3$ at 800 K for (a) Al, (b) Ni, taking into account the whole spectra of attempt frequencies and migration energies, as well as point-defect free energies (the dashed lines indicate the dominant mechanisms of matter transport for each species).

For Al, with diffusion properties strongly composition dependent, the mechanism is of single-sublattice type: for $x_{Ni} > 25\%$, the relevant jumps involve normal Al sites ($8d$ sublattice), whereas $x_{Ni} < 25\%$ induces the emergence of antisite diffusion. $Al(8d) \leftrightarrow Ni(4c)$ jumps, which might be expected to induce coupling between both mechanisms, are not found to contribute, and the efficiency of each [$Al(8d) \leftrightarrow Al(8d)$ or $Ni(4c) \leftrightarrow Ni(4c)$] mechanism may only be lowered by its self-correlation factor.

By contrast, Ni moves essentially via jumps implying $i(4b)$ interstitial sites, either combined with the $Ni(4c)$ sublattice or in a purely interstitial way. While the latter mechanism is a direct consequence of the population of interstitial Ni atoms, the effect of the former may possibly by reduced by correlation effects. The prevalence of the mixed $Ni(4c) \leftrightarrow i(4b)$ mechanism leads to a Ni diffusion tensor almost composition independent. This feature could not be inferred without considering the whole set of possible transitions, which confirms the interest of the current, more comprehensive, approach. This also points out for Ni the possibility (especially for $x_{Ni} > 25\%$) of complex diffusion sequences, alternating $Ni(4c) \leftrightarrow Ni(4c)$ and $Ni(4c) \leftrightarrow i(4b)$ jumps. Refining the picture would imply to take into account cross correlation between both kinds of jumps since the latter must follow each other in a well-defined order. Finally, the main two types of bidefects (complexes) responsible for diffusion, namely, $[V_{Ni(4c)} + Al_{Ni(4c)}]$ and $[V_{Ni(4c)} + Ni_{i(4b)}]$, are found to show negligible binding (<0.03 eV), which suggests the validity of the previous treatment based on one-center defects.

Although the main purpose of the present methodological work was not primarily to yield quantitative information (due to the limits of EAM energy models), it would be useful to confront our approach with tracer diffusion experiments. For the time being, this task is made impossible by the lack of measurements, the only available information concerning interdiffusion.[31] Indeed, whereas theoretical schemes to relate tracer and chemical diffusion have been proposed in more usual (cubic) structures, such attempts for $D0_{11}$ still remain to be performed, complications arising from the anisotropy which requires to define interdiffusion tensors, while most experiments more readily give access to average values. Theoretical refinements are therefore urged, in order to bridge the gap between the increasingly accurate atomic-scale simulations and larger-scale diffusion-controlled properties of materials.

V. CONCLUSION

Considering the case of $NiAl_3$ with $D0_{11}$ cementite structure, the present work was intended to tackle the scarcely explored field of atomic diffusion in ordered compounds with complex structures. Due to the difficulty of carrying out experiments on such compounds, the use of atomic-scale simulations was privileged, an empirical EAM energy model being imposed by the low-symmetry-induced large panel of possible jumps, which still currently rules out more accurate electronic structure calculations. Unexpected features were evidenced, especially the probable role of interstitial defects for diffusion, and the importance of a proper account of the true attempt frequency spectrum, which may drastically invalidate the conclusions inferred from an analysis restricted to jump activation energies. Our analysis furthermore demonstrates the efficiency, in complex ordered phases, of performing a global diffusion analysis without any *a priori* selective discard of transitions. It provides the whole spectra of migration energies and attempt frequencies, namely, all the ingredients entering the various jump rates, which should therefore make it possible, in a near future, to contemplate more realistic correlation- and temperature-dependent simulations in low-symmetry ordered compounds.

*david.tingaud@univ-paris13.fr
†francoise.nardou@unilim.fr
‡Author to whom correspondence should be addressed; remy.besson@univ-lille1.fr

[1] *Intermetallic Compounds: Principles and Practice*, edited by J. H. Westbrook and R. L. Fleischer (Wiley, New York, 1994).
[2] R. Besson, Acta Mater. **58**, 379 (2010).
[3] K. Yamashita, I. Fujimoto, T. Kurakumo, S. Kumai, and A. Sato, Philos. Mag. A **80**, 219 (2000).
[4] P. Yu, C. J. Deng, N. G. Ma, and D. H. L. Ng, J. Mater. Res. **19**, 1187 (2004).
[5] P. Zhu, J. C. M. Li, and C. T. Liu, Mater. Sci. Eng., A **329-331**, 57 (2002).
[6] H. Y. Kim, D. S. Chung, and S. H. Honga, Mater. Sci. Eng., A **396**, 376 (2005).
[7] D. Tingaud, L. Stuppfler, S. Paris, D. Vrel, F. Bernard, C. Penot, and F. Nardou, Int. J. Self-Propag. High-Temp. Synth. **16**, 12 (2007).
[8] R. Saniz, L.-H. Ye, T. Shishidou, and A. J. Freeman, Phys. Rev. B **74**, 014209 (2006).
[9] M. Rasamny, M. Weinert, G. W. Fernando, and R. E. Watson, Phys. Rev. B **64**, 144107 (2001).
[10] D. Tingaud, F. Nardou, and R. Besson, Scr. Mater. **62**, 727 (2010).
[11] O. G. Randl, G. Vogl, and W. Petry, Physica B **219-220**, 499 (1996).
[12] M. Fähnle, G. Bester, and B. Meyer, Scr. Mater. **39**, 1071 (1998).
[13] B. Meyer and M. Fähnle, Phys. Rev. B **60**, 717 (1999).
[14] Y. Mishin, A. Y. Lozovoi, and A. Alavi, Phys. Rev. B **67**, 014201 (2003).
[15] A. Y. Lozovoi and Y. Mishin, Phys. Rev. B **68**, 184113 (2003).
[16] P. Villars and L. Calvert, *Pearson's Handbook of Crystallographic Data for Intermetallic Phases*, 2nd ed. (ASM International, Materials Park, Ohio, 1991).
[17] A. F. Voter and S. P. Chen, in *Characterization of Defects in Materials*, MRS Symposia Proceedings No. 82 (Materials Research Society, Pittsburgh, 1987), p. 175.

[18] M. Ludwig and P. Gumbsch, Modell. Simul. Mater. Sci. Eng. **3**, 533 (1995).
[19] M. Yan, V. Vitek, and S. P. Chen, Acta Mater. **44**, 4351 (1996).
[20] Y. Mishin, M. J. Mehl, and D. A. Papaconstantopoulos, Phys. Rev. B **65**, 224114 (2002).
[21] C. L. Fu, Y.-Y. Ye, M. H. Yoo, and K. M. Ho, Phys. Rev. B **48**, 6712 (1993).
[22] B. Meyer and M. Fähnle, Phys. Rev. B **59**, 6072 (1999).
[23] D. Tingaud and R. Besson, Phys. Status Solidi C **6**, 2008 (2009).
[24] G. Henkelman and H. Jonsson, J. Chem. Phys. **113**, 9978 (2000).
[25] V. Schott, M. Fähnle, and P. A. Madden, J. Phys.: Condens. Matter **12**, 1171 (2000).
[26] D. Tingaud, Ph.D. thesis, Université de Limoges, 2006.
[27] R. Besson, A. Legris, and J. Morillo, Phys. Rev. B **74**, 094103 (2006).
[28] N. Chetty, M. Weinert, T. S. Rahman, and J. W. Davenport, Phys. Rev. B **52**, 6313 (1995).
[29] G. Henkelman, B. Uberuaga, and H. Jonsson, J. Chem. Phys. **113**, 9901 (2000).
[30] R. Besson, S. Guyot, and A. Legris, Phys. Rev. B **75**, 054105 (2007).
[31] *Diffusion Processes in Ordered Alloys*, edited by L. N. Larikov, V. V. Geichenko, and V. M. Fal'chenko (Oxonian Press, New Dehli, 1981).